Hindawi
International Journal of Rotating Machinery
Volume 2021, Article ID 5582509, 13 pages
https://doi.org/10.1155/2021/5582509

Research Article

Effects of Side Load Chains of a Combine Harvester on Unbalanced Dynamic Vibrations of Its Threshing Drum

Yu Zhiwu, Li Yaoming, Wang Xinzhong, Tang Zhong, and Jiahui Lu

Key Laboratory of Modern Agricultural Equipment and Technology, Ministry of Education, Jiangsu University, Zhenjiang, 212013 Jiangsu, China

Correspondence should be addressed to Li Yaoming; ymli@ujs.edu.cn

Received 30 January 2021; Accepted 11 April 2021; Published 30 June 2021

Academic Editor: Ashwani K. Gupta

In order to study the influence of the side drive on the balance state of the threshing drum, this paper used the side eccentric load chain drive as the power on the threshing drum dynamic balance test bench. By analyzing the influence of different radial phases, different axial distances, and spiral combinations of the threshing drum on the counterweight, this paper studies the law of the effect of side partial load chain drive on the dynamic balance of the threshing drum and finds that the side chain drive has obvious influence on the unbalance phase of the threshing drum and the change of the axial distance of unbalance has little effect on the equilibrium state of the threshing drum. And from this, a vibration balance method based on the equivalent unbalance of the chain drive is proposed, which can predict and calculate the unbalance of the threshing drum. The unbalance of the threshing drum predicted by this method is smaller than the actual measured unbalance. The maximum error is 32.64% and the minimum error is 4.6%. In the two tests, the predicted unbalance is 1.24 mm/s in amplitude and 270 degrees in phase and amplitude 1.4 mm/s and phase 120 degrees, respectively. The measured unbalance is amplitude 1.587 mm/s and phases 286 degrees. The error between prediction and actual measurement is less than 32.64%, and the unbalance amplitudes that can be reduced by one-time dynamic balance are 0.856 mm/s and 0.674 mm/s, respectively. The research results in this paper provide an effective method for the balance state of the multidrum side chain transmission.

1. Introduction

Rotating machinery is widely used in agricultural machinery. Studies have shown that 70% of the vibration problems of rotating machinery are caused by dynamic balance problems. The unbalance of rotating machinery will cause bearing wear, shaft deformation, and cracks and reduce the service life of parts, produce vibration and noise, and affect the reliability of the whole machine [1]. The threshing drum is the main working part of the combine harvester for threshing and separation. The working speed is high, and the dynamic balance is usually carried out on the dynamic balance machine before assembly. However, the dynamic balance machine cannot ensure that the supporting state is completely the same as that of the machine, and the boundary conditions of the rotor are changed after assembly. At the same time, it is affected by the transmission components, so the rotor will produce new imbalance when it is running. On-site dynamic balancing technology is the dynamic balancing technology of the rotor on its own bearing and frame, rather than on the dynamic balancing machine. The stones in the threshing gap often cause the deformation of the rack bar of the threshing drum and the wear of the rack. After the rack is replaced, the dynamic balance state of the rotor changes. The on-site dynamic balance technology does not need to disassemble the rotor. The rotor dynamic balance correction can be completed on the whole machine, which plays an important role in the later inspection and maintenance of the equipment [2].

There are many rotating parts in the combine harvester, such as the threshing drum, fan, reel, auger, and other key working parts [3], and its transmission mode is mainly belt transmission and chain transmission [4]. The dynamic balancing method of the transmission only considers the vibration characteristics of the unbalance of the rotary part itself, which has a good balance effect for the rotary part directly driven by the axis. However, the belt and chain drives

are both side-biased load drives, and the impact on the unbalanced response of the rotating parts is more reflected in the phase [5]. The traditional dynamic balancing method often ignores the influence of the transmission on the unbalanced characteristics, which will lead to poor balance effect and the remaining unbalanced amount cannot reach the requirements. Because the influence of the shaft and the bearing is generally not considered when studying the transmission and when studying the rotor system, the traditional method often treats the transmission as a rigid disk; regardless of the influence of the transmission, each rotor is designed separately, and bending vibration and torsional vibration are also calculated separately. In the multirotor system with transmission, due to the transmission meshing, the bending vibration and torsional vibration of each rotor are coupled, and the transmission, bearing, and rotor have become an integral part of the system [6].

At present, many scholars have made great achievements in rotor system modeling, rotor system unbalance response analysis, rotor dynamic balance methods, etc., focusing on rotor dynamic balance vibration and other issues. Polushkin et al. [7] studied the influence of unbalance in the correction planes of the part on the vibrations of its bearing in the balancing machine. Tang et al. [8] revealed the inherent characteristics and dynamic response of unbalanced vibration through the axial trajectory and axial vibration of the threshing drum. [9] analyzed the coupled vibration of the shaft support system. Yao et al. [10] applied the harmonic response analysis method to study the unbalanced vibration response of the turbine generator rotor. Wang et al. [11] studied the use of finite element methods to study the unbalanced response of cracked rotors. Tiwari et al. [12] conducted a nonlinear dynamic analysis of the rigid rotor supported by ball bearings. Zhao et al. [13] proposed an analytical method to study the coupling dynamic characteristics of four unbalanced rotors. Liu et al. [14] proposed an improved dynamic model of ACBB to consider the influences of elastic hysteresis, differential sliding friction torques, and elastohydrodynamic lubrication (EHL) rolling on the ball motion state. Zhao et al. [15] proposed a transient characteristic-based balancing method (TCBM) combined with dynamic load identification (DLI) technique to identify the unbalance parameters of the general rotor system. Shin et al. [16] presented a novel approach for modeling and analyzing a geared rotor-bearing system including nonlinear forces in the gear set and the supporting fluid film journal bearings.

More and more scholars have begun to pay attention to the vibration balance of rotary parts and have made great achievements in vibration analysis of transmission methods, dynamic modeling of transmission systems and rotary parts, and dynamic balancing methods of axial direct transmission. For example, [5] established a lateral vibration model of the chain drive and pointed out that when the chain is excited on one side, the chain resonates obviously at its natural frequencies of each order. Based on the belt transmission vibration model, [17] proposed a solution method for the tension of the belt on both sides of the tension wheel to the mass moment of the particle and established a pass calculation model for the rotational vibration of the attachment system of the multiribbed belt. Liu et al. [18] established a dynamic model of the toothed chain timing transmission system based on the coupled vibration response of the engine and conducted an experimental study on the dynamic tension of the transmission system chain. Donley et al. [19] used the finite element method to establish a dynamic model of a gear transmission rotor system. Lee and Ha [20] have carried out dynamic modeling analysis for gear-coupled parallel rotor system. Sun et al. [21] proposed a method without trial based on the unbalance identification and modal analysis of the finite element dynamic model of the high-speed spindle system based on the principle of "modal force equivalent." Yang et al. [22] studied a general method for predicting the unbalanced response of the gear rotor system. On this basis, a method for calculating the maximum shaft radius of the unbalanced response of the gear rotor system was proposed. Effects of the fault width, moment, and input speed on the time- and frequency-domain responses of the planetary gear were analyzed [23]. Alves et al.'s [24] research had shown that characteristics of oil film nonlinearity in bearings could seriously affect the possibility of balancing with the use of influence coefficients. The above studies consider the vibration of the transmission and the slewing body, respectively, and mainly carry out related research on the force of the transmission system by means of simulation modeling.

However, the vibration inducement of the slewing body is not only the tension on the transmission belt and chain [25] but also the lateral vibration during operation [26]. The vibration response of the slewing body due to the belt drive and chain drive will also affect the fundamental frequency vibration, inducing the unbalanced state of the slewing part. The chain drive is widely used in the combine harvester. The chain wheel and sprocket are prone to produce violent meshing impact vibration. The lateral vibration of the chain itself will produce a large dynamic load, which will aggravate the chain shaking and the vibration of the working parts impact [27]. Yang et al. [22] studied the influence of the belt on the development of the balance system and analyzed the influence of the lateral vibration of the belt on the transmission system. Li et al. [28] used the harmonic balance method to solve the frequency response curve of the belt drive system. Based on discrete mathematics, Bazhenov et al. [29] studied the parametric resonance of elastic systems under periodic and stochastic loads. Wang [30] test results show that periodic torsional oscillations of engine camshafts induced by power train loads can cause significant tension variation in the timing chain and magnify the chain transverse vibrations and noise level.

In the combine harvester, the transmission path of the threshing drum is complex. The vibration of the transmission parts and the impact and winding of the material on the threshing drum will affect the balance state of the entire drum and thus the balance state between the transmission part and the threshing drum [31–33]. In this paper, the effect of the side chain drive and random weight on the dynamic balance of the threshing drum is studied, and on this basis, the unbalance of the threshing drum is predicted, and a dynamic balancing method based on the side eccentric load chain drive threshing drum is proposed.

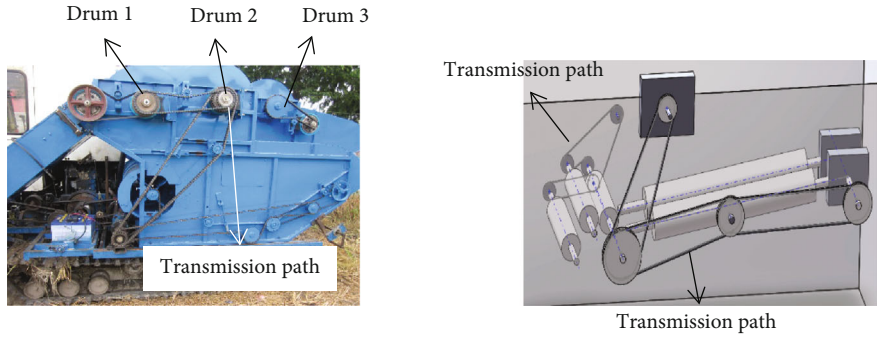

Figure 1: Schematic diagram of multiroller side transmission.

2. Material and Methods

2.1. Establish Multidrum Test Bench. There are many combinations of threshing rollers of the combine harvester, including dual longitudinal axial flow rollers, single-cutting single longitudinal flow rollers, and combinations of multiple-cutting rollers, such as the double-cut single longitudinal flow combination of the German CALAAS Harvester and three-cut dual-longitudinal-flow combine harvester of Deere. Different drum combinations have different transmission methods. Chain transmission, belt transmission, and gear transmission are all applied, either a single transmission method or a mixture of multiple transmission methods. The schematic diagram of multiroller side transmission is shown in Figure 1.

Due to the multiple vibration sources of the combine harvester and the complicated transmission path, the power needs to be transmitted from the engine to the threshing drum after multiple transmissions. There are too many interference factors on the way, so it is not convenient to study the chain drive on the whole machine to balance the threshing drum impact. Therefore, according to the characteristics of the threshing drum and its power transmission path, the dynamic balancing test bench of the threshing drum is designed, so as to reduce the interference of external influence factors on the test results. The dynamic balancing test bench of the threshing drum is shown in Figure 2.

The threshing drum dynamic balance test bench designed in this paper is 1390 mm long, 974 mm wide, and 1006 mm high. Six threshing drums of the same size are arranged in parallel on the test bench and can be driven on both sides to achieve multiple transmission paths, and the speed is adjustable from 0 to 1000 rpm. The whole frame is smooth, which is convenient for installing various sensors with magnetic table base for vibration test. The test bench can simulate various working conditions of the threshing drum, which is convenient for testing the dynamic balance of the threshing drum under different working conditions. The three-dimensional structure of the threshing drum is shown in Figure 3.

The three-dimensional structure of the threshing drum is shown in Figure 3, with a diameter of 240 mm and a length of 612 mm, which are all scaled in proportion to the size of the conventional threshing drum on the combine harvester. There are 6 counterweight holes on the two sides of the threshing drum, evenly distributed at an angle of 60. There are 10 counterweight holes on each rack, 5 counterweight holes are distributed between the two sides of the wheel and the middle wheel at 50 mm intervals, and the diameter of all counterweight holes in the drum is 8.5 mm, which is convenient for adding weights.

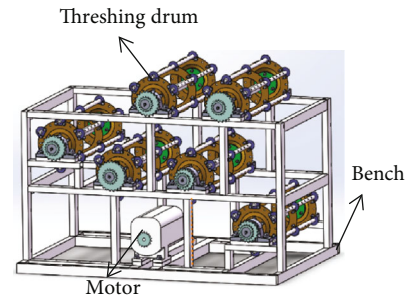

Figure 2: Threshing drum dynamic balance test bench.

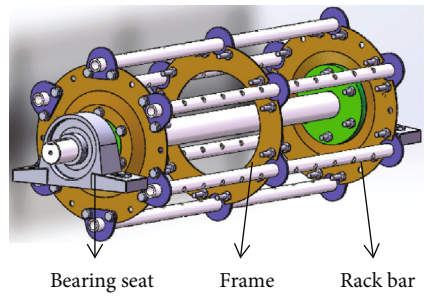

Figure 3: Three-dimensional structure of the threshing drum.

2.2. Modal Analysis of Threshing Drum. Finite element modal analysis first needs to establish the geometric model of the structure in SOLIDWORKS, save the geometric model in STEP format, import it into ANSYS Workbench software, and set the material parameters. The material of the threshing drum part of the combine harvester is mainly Q235, query the density, Poisson's ratio, yield strength, modulus of elasticity of materials, and input them into ANSYS.

Finite element analysis is to idealize the continuum as a collection of a limited number of elements, which are

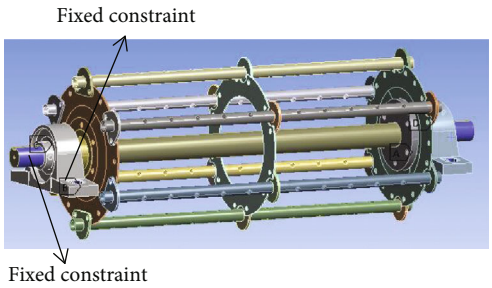

Figure 4: Threshing drum constraint model.

connected only at a limited number of nodes. The nodes are generally on the boundary of the elements, and the elements are connected by nodes and bear a certain load to form a finite element assembly. On this basis, a simple displacement function is assumed for each element to approximate its displacement distribution law, the equilibrium equation of each element is obtained through the principle of virtual work displacement, and the relationship between the element nodal force and nodal displacement is established. Finally, the characteristic relations of all the elements are assembled, the boundary constraint conditions are introduced, the equations are solved to obtain the nodal displacement, and the stress of each element is calculated.

Then, the research object is discretized into a collection of grid-like block regions. Correct division of the number and density of the grid can reduce the calculation time and improve the simulation effect. The grid division of the threshing drum is automatically selected, and the grid division method can be automatically selected according to the shape of the entity. The threshing roller is installed on the frame through the bearing seat, therefore, its tangential free and radial and axial constraints; the constraint model is shown in Figure 4.

2.3. Dynamic Balance Instrument and Test Method. Use S956Y-1 portable dynamic balance instrument, acceleration sensor, and photoelectric speed sensor to test on the threshing drum test bench. The test instrument is shown in Figure 5, and the main performance parameters are shown in Table 1.

First, an acceleration sensor and a photoelectric speed sensor are arranged on the driving surface of the threshing drum. The test found that the unbalance in the horizontal direction is greater than the unbalance in the vertical direction, so the vibration sensor is installed in the horizontal direction of the bearing housing. The installation of the photoelectric speed sensor needs to stick a reflective strip (phase zero mark) on the threshing drum's wheel to adjust the position of the photoelectric sensor so that the light spot of the sensor can hit the reflective strip. In the test, the weights of different phases in the radial direction of the end surface of the threshing drum, the weights in different distances in the axial direction of the end surface, and the radial and axial spiral weights are used to balance the weight. The unbalance of threshing drum is produced by using counterweight and tested. The acceleration corresponding to the frequency of the drum at the working speed is measured by using acceleration vibration sensor as the unbalance amplitude of the drum.

3. Results and Discussion

3.1. Modal Analysis of Threshing Drum. ANSYS Workbench is used to solve the constraint mode and vibration mode of the frame. The simulation results of the first and second critical speeds are shown in Figure 5.

The frequency of the first six modes of the threshing drum is shown in Table 2.

It can be seen from Table 2 and Figure 5 that the natural frequencies of the first two stages of the threshing drum are very close. The natural frequencies of the first stage and the second stage correspond to the local modes of the intermediate disc. The natural frequencies of the first stage are 143.76 Hz, the critical speed is 8625.6 RPM, and the normal working speed of the threshing drum is 600-1000 RPM. Therefore, the first critical speed of the threshing drum is much higher than the normal working speed, which completely avoids the resonance, and the vibration measured in the test is not affected by the resonance of the threshing drum.

3.2. Influence of Counterweight on Dynamic Balance of Chain Drive Drum. In order to study the dynamic unbalance law of the side chain drive caused by the random balance weight, the driven drum which is powered by the side chain drive is selected as the research object, and the dynamic balance change of the driven drum is studied by the random balance weight on the drum. Before the test, the initial dynamic balance of the driven drum is carried out to reduce the initial unbalance of the drum and the interference to the subsequent test.

Because the speed of the threshing drum is 600~1000 rpm, the speed will decrease after being winded and impacted by materials, about 700 rpm. Therefore, the speed of the active drum and the driven drum is 700 rpm, which is consistent with the actual working condition.

The initial unbalance amplitude of the driven drum is 1.234 mm/s and the phase is 159. The test weight is related to the rotor mass, the weighted radius, and the balance speed. According to the data displayed by the dynamic balance instrument, it is necessary to add 82.03-164 g of test weight, 107.7 g of actual test weight, and 90 degrees of test angle. After weighting, the amplitude of unbalance is 0.562 mm/s and the phase is 204 degrees, so it is suggested to add 143.4 g counterweight on the 115-degree phase. Due to the influence of counterweight position, 142.45 g counterweight is added on the 120 phases, the measured residual unbalance amplitude is 0.37 mm/s, the phase is 161, and the amplitude is reduced by 70%, reaching the highest standard of balance grade ISO 1940, G0.4.

At the same time, 58.8 g mass block is added in the 240° direction of the roller to artificially make the roller unbalanced. According to the parallelogram rule of vector calculation, the angle of the weighted unbalance is between 161° of the initial unbalance phases and 240° of the weighted phase.

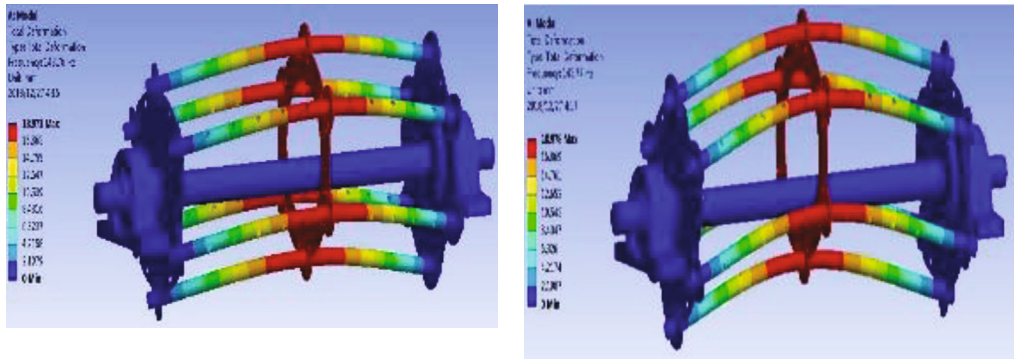

(a) First-order modal (b) Second-order modal

(c) Third-order modal (d) Fourth-order modal

Figure 5: Modal shape of threshing drum.

Table 1: Main performance parameters of test instruments.

Device name	Performance	Parameter value	Factory
S956Y-1 portable dynamic balancer	Frequency range (Hz)	10~5000	Beijing Sundege Technology Company
	Frequency response error (%)	±5	
	Maximum range (mm/s)	100	
	Highest resolution (mm/s)	0.1	
L14A piezoelectric acceleration sensor	Sensitivity (pc/ms^{-2})	3.5~5.2	
	Frequency range (Hz)	2~3000	
	Max acceleration (m/s^2)	2000	
SGD-1-5V photoelectric speed sensor	Measuring range (rpm)	1~60000	
	Operating voltage (Vdc)	5	
	Output signal	TTL pulse signal	

Table 2: Constrained mode of the threshing drum.

Modal order	Frequency (Hz)	Critical speed (rpm)
1	143.76	8625.60
2	143.77	8626.20
3	197.05	11823
4	293.1	17586
5	298.33	17899.80
6	198.41	11904.60

However, at the same speed, the actual measured phase of the weighted unbalance is 108°, and the phase relationship is shown in Figure 6. It can be seen from this phase change that

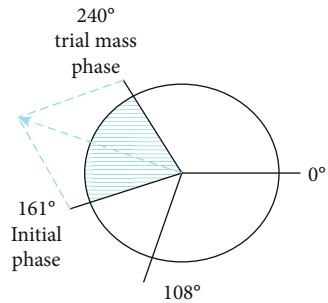

Figure 6: Unbalance phase relationship diagram.

the side chain drive will affect the unbalanced state of the threshing roller.

3.2.1. End Face Radial Different Phase Counterweight. The end face phase of the threshing drum is shown in Figure 6. The rotation direction of the threshing drum is counterclockwise, so the reflective strip is positive clockwise (Figure 7), and the wrapping angle of the chain drive is in the range of 90-270°.

Since the dynamic balance of driven drum has been carried out on site before the test, the driven drum can be regarded as absolute balance. The actual measured unbalance is caused by chain drive unbalance and counterweight quality. Chain drive unbalance (OA) + trial mass unbalance (OB) = actual measured unbalance (OC).

Set the unbalance of chain drive as OA = (x_A, y_A), and the trial mass unbalance is OB = (x_B, y_B). Its amplitude is L_B. The added phase of the mass block is α. The actual measured unbalance is OC = (x_C, y_C). During the test, 161.3 g masses were added to the counterweight holes in the direction of the end face of the threshing drum 60°, 120°, 180°, 240°, 300°, and 360° in order to measure the unbalance of the threshing drum. The test data is shown in Table 3, and the phase change area is shown in Figure 8.

Because the threshing drum rotates counterclockwise, the loose edge of the chain drive is up and the tight edge is down. There is tension on the sprocket by the chain, and the loose edge will produce a certain impact force and axial force on the sprocket, especially the tension of the drive chain. When the transmission chain is not sufficiently tensioned, the lateral vibration of the chain is obvious, so the vibration generated by the chain transmission at the critical point of the angle of 90 degrees and 270 degrees is large. Therefore, the unbalance effect of the chain drive on the drum can be equivalent to two unbalanced quantities, and it can be changed according to the change of the unbalance condition of the threshing drum.

Select the data when the rotation speed is 700 rpm, calculated from the data in Table 3.

At 60°, OB = $(L_B \cos 60°, L_B \sin 60°)$, OC = (0.426 cos 275°, 0.426 sin 275°).

At 120°, OB = $(-L_B \cos 60°, L_B \sin 60°)$, OC = (0.502 cos 135°, 0.502 sin 135°).

At 180°, OB = $(-L_B, 0)$, OC = (0.382 cos 124°, 0.382 sin 124°).

At 240°, OB = $(-L_B \cos 60°, -L_B \sin 60°)$, OC = (0.513 cos 173°,0.513 sin 173°).

At 300°, OB = $(-L_B \cos 60°, L_B \sin 60°)$, OC = (0.483 cos 209°, 0.483 sin 209°).

At 360°, OB = $(L_B, 0)$, OC = (0.465 cos 256°, 0.465 sin 256°).

Available from the formula OA + OB = OC

$$\begin{cases} x_A = x_C - x_B, \\ y_A = y_C - y_B. \end{cases} \tag{1}$$

The angle range of the transmission chain is 90~270 degrees, so $x_A < 0$.

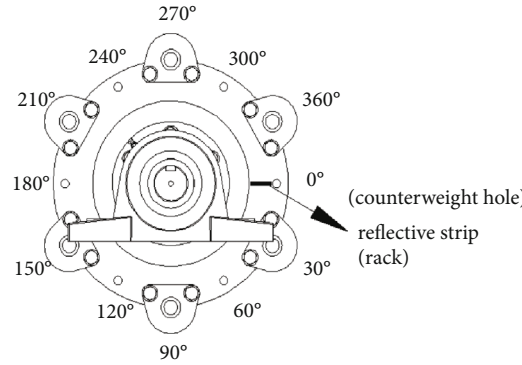

Figure 7: Schematic diagram of the end face of the threshing drum.

Solving the inequality group can obtain $0.074 < L_B < 0.214$, and substitute equation (1) to obtain the variation range of the chain transmission unbalance amount (OA) at various angles. The variation range of the chain transmission unbalance is shown in Figure 9.

The mass of an unbalanced rotor can be expressed by the following equation:

$$m = \int_L \mu(x, y) ds, \tag{2}$$

where $\mu(x, y)$ is linear density.

Because the rotor in the range of wrap angle is affected by the chain drive to varying degrees, there is an unbalanced mass, and the unbalance is uneven and varies in size. Therefore, according to the idea of "divide first, and then sum," all the unbalance produced in the process of chain transmission can be equivalent to two unbalances, namely, the influence of tight edge (OA_1) and loose edge (OA_2) on the drum unbalance. The unbalance of chain drive is composed of these two unbalance quantities $OA_1 + OA_2 = OA$.

According to the actual engagement of the test-bed sprocket and the phase distribution of the unbalance of the chain drive, set the unbalance of tight side of chain drive as $OA_1 = (x_A, y_A)$, its amplitude is L_{A_1}, and the phase angle is 105 degrees.

$$\begin{cases} x_{A_1} = -L_{A_1} \sin 15°, \\ y_{A_1} = -L_{A_1} \cos 15°. \end{cases} \tag{3}$$

The unbalance of loose edge is $OA_2 = (x_A, y_A)$, its amplitude is L_{A_2}, and the phase angle is 270 degrees.

$$\begin{cases} x_{A_2} = 0, \\ y_{A_2} = L_{A_2}. \end{cases} \tag{4}$$

From the coordinate expression of vector OA + OB = OC , we can get

$$\begin{cases} x_{A_1} + x_{A_2} = x_A = x_C - x_B, \\ y_{A_1} + y_{A_2} = y_A = y_C - y_B. \end{cases} \tag{5}$$

Table 3: Unbalanced amount of each phase point.

Rotating speed (rpm)	60 degrees		120 degrees		180 degrees		240 degrees		300 degrees		360 degrees	
	Amplitude (mm/s)	Phase (°)	Amplitude (mm/s)	Phase (°)	Amplitude (mm/s)	Phase (°)	Amplitude (mm/s)	Phase (°)	Amplitude (mm/s)	Phase (°)	Amplitude (mm/s)	Phase (°)
600	0.532	222	0.431	146	0.220	135	0.383	181	0.631	186	0.618	214
700	0.426	275	0.502	135	0.382	124	0.513	173	0.483	209	0.465	256
800	0.486	319	0.735	127	0.538	102	0.972	161	0.661	219	0.622	268
900	1.160	27	1.869	121	2.028	114	1.487	159	1.271	180	0.861	341
1000	1.716	35	2.662	112	2.868	123	2.725	149	1.863	163	1.094	30

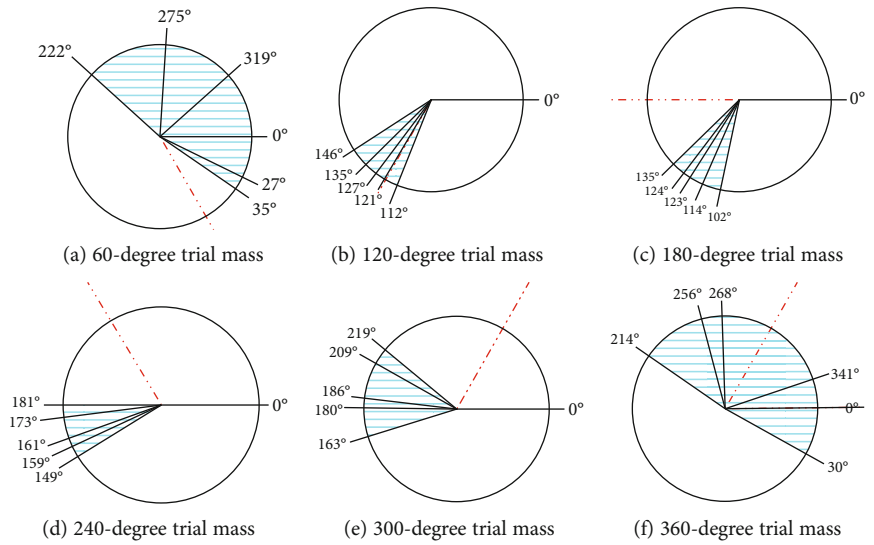

(a) 60-degree trial mass (b) 120-degree trial mass (c) 180-degree trial mass

(d) 240-degree trial mass (e) 300-degree trial mass (f) 360-degree trial mass

Figure 8: End face radial weight unbalance phase change zone.

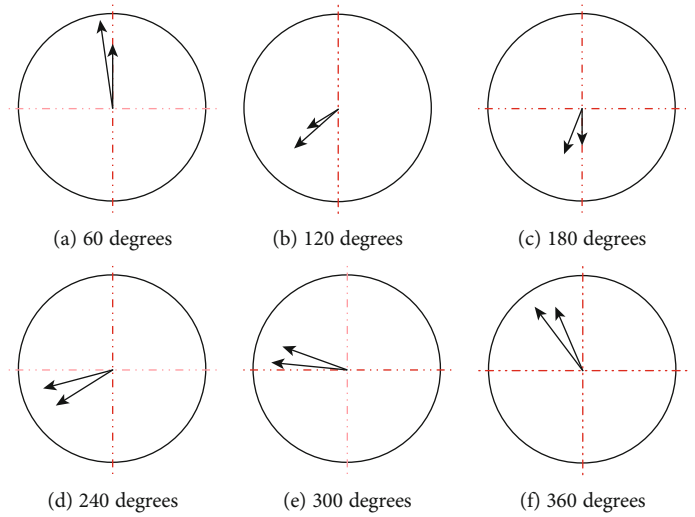

(a) 60 degrees (b) 120 degrees (c) 180 degrees

(d) 240 degrees (e) 300 degrees (f) 360 degrees

Figure 9: Schematic diagram of the range of variation of the chain drive unbalance.

By substituting equations (3) and (4) into equation (5), we can get

$$\begin{cases} L_{A_1} = \dfrac{x_C - x_B}{-\sin 15^\circ}, \\ L_{A_2} = y_C - y_B + L_{A_1} \cos 15^\circ, \end{cases} \tag{6}$$

where the x_C, y_C is known quantity and OB is a function of L_B,

$$\mathrm{OB} = \begin{cases} (L_B \cos \alpha, -L_B \sin \alpha), \text{else}, \\ (L_B \sin \alpha, -L_B \cos \alpha), \alpha \in (180^\circ, 270^\circ). \end{cases} \tag{7}$$

The calculation can get $0 < L_{A_1} < 2.04$ and $0 < L_{A_2} < 2.58$.

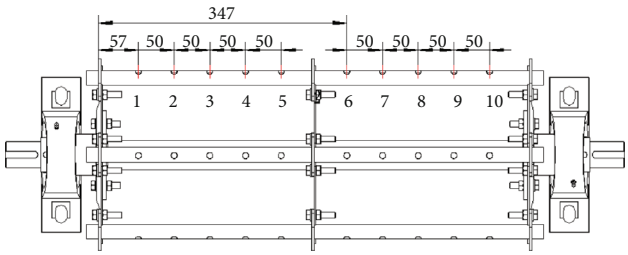

Figure 10: Schematic diagram of the axial weight hole of the threshing drum.

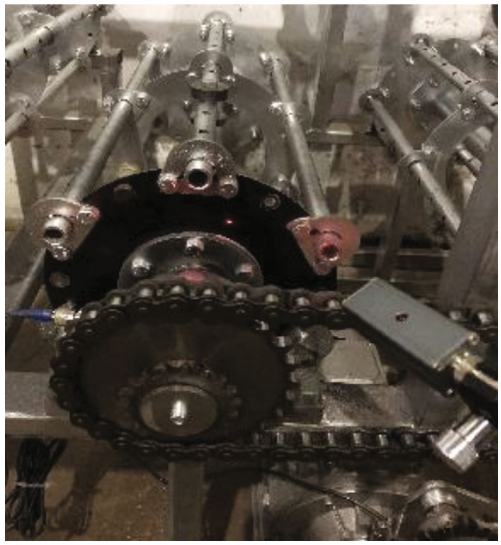

Figure 11: End face axial distance different weights.

3.2.2. End Face Axial Weights at Different Distances. The schematic diagram of the axial counterweight holes on the end surface of the threshing drum is shown in Figure 10. In the experiment, at different speeds, select the gear rods in the three directions of 90 degrees, 150 degrees, and 210 degrees on the driven roller, add 161.3 g masses to the different weight holes in sequence, and measure the unbalance of the drum, such as shown in Figure 11; the test data is shown in Table 4.

The severe lateral vibration of the chain drive during high-speed operation is the main reason for the instability of the high-speed chain drive system. Therefore, high-speed operation will increase the amplitude of the chain drive unbalance (OA), that is, the amplitude of the unbalance of the threshing drum (OC), so the higher the speed, the greater the unbalance amplitude.

According to the dynamic balance equation of the rigid rotor,

$$\begin{cases} \int u(z)dz + \sum_{i=0}^{N} W_i = 0, \\ \int u(z)zdz + \sum_{i=0}^{M} W_i z_i = 0, \end{cases} \tag{8}$$

where $u(z)$ is the random space vector, W_i is the correction in x and y directions, and z_i is the axial coordinate of the correction.

Among the dynamic balance equations, the first formula is the force balance equation, and the second formula is the force couple balance equation. It can be seen from the system of equations that there is a unique solution only when $N = 2$, so although $u(z)$ is a random space vector, only two corrections are required. The dynamic balance equation does not require the axial position of the correction, that is, the change of the axial distance has little effect on the change of the unbalance. However, from the test data in Table 4, it can be seen that when the threshing drum is running at a high speed, adding the weights in holes 6 to 10 will significantly increase the unbalanced amplitude of the threshing drum.

According to the differential equation of motion of a single degree of freedom torsional vibration system,

$$J\ddot{\theta} + c_\theta\dot{\theta} + k_\theta\theta = M_{(t)}, \tag{9}$$

where J is the rotational inertia of disc, $J = mr^2$, where m is the Rigid body mass and r is the radius of gyration, θ is the angular displacement of the disc at a certain moment, $c_\theta\dot{\theta}$ is the damping torque, $k_\theta\theta$ is the elastic recovery torque, and $M_{(t)}$ is the excitation torque.

Add weights to holes 6 to 10 in the threshing drum, and the distance between it and the front disc is getting farther and farther; the radius of rotation r of the rotational inertia is different. And the farther r is, the greater the moment of inertia generated, the greater the excitation torque. The front end of the threshing drum is the transmission end, and the unbalance of the chain drive increases under high-speed operation, and the rear end is close to the counterweight. The excitation torque received increases. Under the joint action of the two, the unbalanced amplitude of the threshing drum increases great such as shown in Figure 12.

Above all, when the speed of the threshing drum is lower than 800 rpm, the change in the distance of the added weights has little effect on the unbalance of the drum and the amplitude is stable. When the rotation speed is higher than 800 rpm, the change of the distance of the counterweight has a great influence on the drum unbalance. Taking hole 6 as the critical point, adding weight to the second half of the entire drum, namely, holes 6 to 10, the unbalanced amplitude of the threshing drum is large, and this change is particularly obvious as the speed increases as shown in the Figure 13.

3.2.3. Radial and Axial Spiral Weights. The spiral weight is to add mass blocks of equal mass to the weight holes of different distances on the rack bar of different phases of the threshing drum at the same time and comprehensively consider the influence of the two factors of the weight phase and the weight distance on the unbalance of the threshing drum. During the test, add a mass of 77.05 g to the 1st hole of the 30-degree rack, 77.17 g at the 2nd hole of the 90-degree rack bar, 76.8 g at the 3rd hole of the 150-degree rack bar, 77.1 g at the 4th hole of the 210-degree rack, 76.27 g at the 5th hole of the 270-degree rack bar, 75.49 g at the 6th hole of the 330-

Table 4: Unbalance amplitude of each weight hole at different speeds (mm/s).

Hole number	90 degrees					150 degrees					210 degrees				
	600 rpm	700 rpm	800 rpm	900 rpm	1000 rpm	600 rpm	700 rpm	800 rpm	900 rpm	1000 rpm	600 rpm	700 rpm	800 rpm	900 rpm	1000 rpm
1	0.196	0.461	0.586	1.665	2.577	0.545	0.903	1.98	1.476	2.489	0.379	0.590	0.935	2.274	2.403
2	0.179	0.492	0.632	1.952	2.399	0.619	1.222	1.844	3.030	4.337	0.334	0.446	1.112	1.467	2.915
3	0.177	0.374	0.784	1.905	2.207	0.407	1.518	2.356	3.969	4.911	0.415	0.481	0.733	1.744	2.565
4	0.129	0.631	0.764	1.391	2.32	0.416	1.728	1.825	3.782	4.367	0.302	0.350	0.647	1.353	2.073
5	0.089	0.517	0.739	1.874	2.232	0.782	1.478	2.704	4.157	4.760	0.439	0.383	0.673	1.739	1.909
6	0.232	0.657	0.954	2.011	4.452	0.601	1.314	2.212	3.225	3.992	0.278	0.317	0.501	1.182	2.129
7	0.190	0.697	1.166	2.533	3.459	0.287	1.33	2.478	3.886	7.084	0.296	0.307	0.490	1.530	1.965
8	0.142	0.656	0.981	3.109	3.416	0.477	1.543	1.778	3.475	4.615	0.233	0.232	0.813	1.301	1.915
9	0.155	0.450	1.067	2.351	3.753	0.467	1.807	2.343	3.527	4.456	0.263	0.291	0.545	1.149	2.183
10	0.158	0.639	1.218	2.907	3.360	0.366	0.757	2.814	3.419	4.980	0.195	0.262	0.500	1.540	1.983

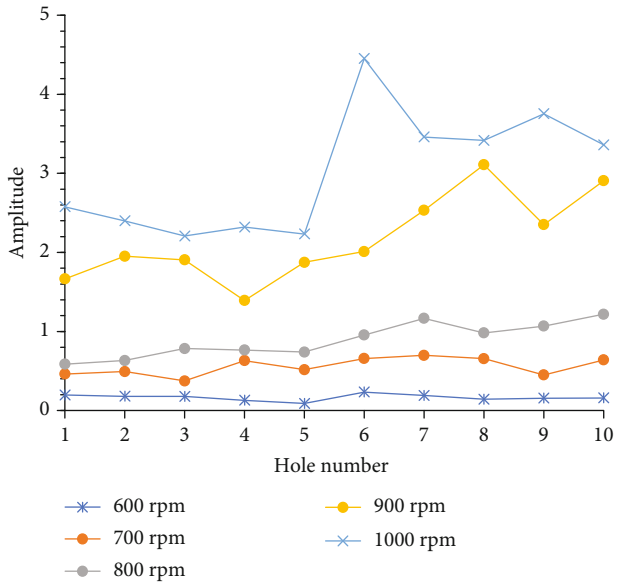

Figure 12: 90-degree toothed rod variable distance weight-amplitude map.

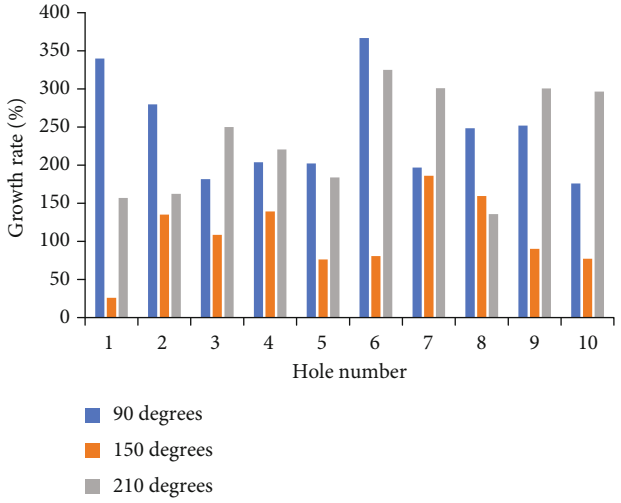

Figure 13: Each weight hole 800~1000 rpm amplitude increase.

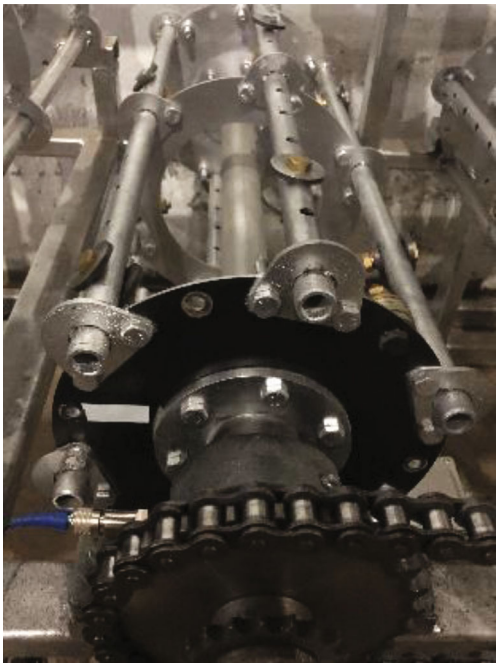

Figure 14: Schematic diagram of spiral weight.

Table 5: Unbalance of the threshing drum under the spiral counterweight.

Rotating speed (rpm)	Amplitude (mm/s)	Phase (°)
600	0.216	163
700	0.234	20
800	3.378	59
900	4.122	67
1000	5.624	102

degree rack bar, 75.15 g for the 7th hole of the 30-degree rack, 76.78 g for the 8th hole of the 90-degree rack, 73.9 g for the 9th hole of the 150-degree rack, and 74.67 g for the 10th hole of the 210-degree rack. The position of the spiral counterweight is shown in Figure 14. The measured test data is shown in Table 5.

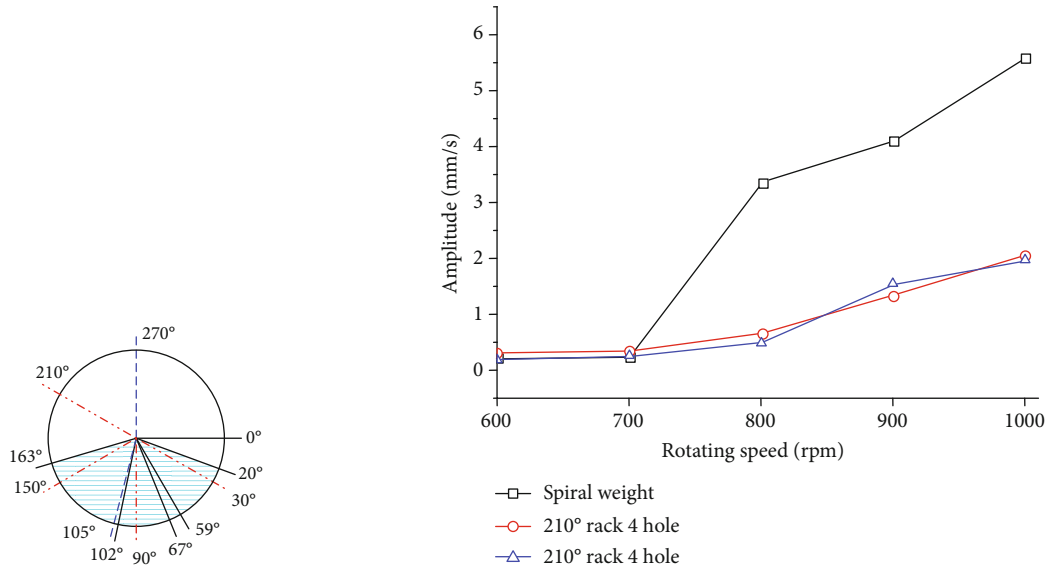

(a) Schematic diagram of spiral trial mass weight phase (b) Comparison of amplitude between spiral weight and variable distance weight

Figure 15: Analysis of unbalance of spiral weight.

From the above test, it can be seen that when adding a mass in a variable phase, the phase of the unbalance of the threshing drum will always be concentrated near the phase of the equivalent unbalance of the chain drive and the phase of the mass. When adding masses at variable distances, the amplitude of the unbalance of the high-speed threshing drum will increase significantly. Two sets of masses are added to the gear rods in the helical directions of 30 degrees, 90 degrees, 150 degrees, and 210 degrees, and only one set of masses is added to the tooth rods in the directions of 270 degrees and 330 degrees. The phase of the chain drive equivalent unbalance is 105 degrees and 270 degrees, so the phase of the unbalance value of the threshing drum is in the area shown in Figure 15(a). In addition, when the counterweight is used, masses are added to the counterweight holes at different distances of the racks of different angles, so the amplitude measured is much larger than the amplitude when a single mass is added, and the amplitude at 800 rpm increase rapidly, as shown in Figure 15(b).

3.3. Field Dynamic Balancing of Threshing Drum. The variation range of the actual unbalance (OC) can be calculated from the equivalent unbalance of the chain drive (OA) and the unbalance of the trial mass (OB). In the test, the balance speed was selected as 700 rpm for the active drum and 500 rpm for the driven drum, and the counterweights were added to the holes 1 and 2 of the 270-degree and 30-degree rack bar of the driven drum, respectively, and the variation range was calculated. Select a certain phase within its range, add a mass in the opposite direction of the end surface of the threshing drum to balance, and measure the remaining unbalance.

During low speed balancing, the phase difference between the trial mass phase and the unbalance is generally greater than 90 degrees. Since the amplitude of the boundary unbalance is the maximum amplitude, half of the maximum amplitude is selected to calculate the counterweight. If the vibration reduction effect is not good, appropriately increase the weight of counterweight.

In the first set of experiments, add 161.3 g of trial mass to the 1st hole in the 30-degree direction of the threshing drum, $\mathrm{OB} = (0.866L_B, 0.5L_B)$.

From formulas (4), (5), and (6),

$$\begin{cases} x_C = 0.866L_B - L_{A_1} \sin 15^\circ, \\ y_C = -0.5L_B - L_{A_1} \cos 15^\circ + L_{A_2}, \end{cases} \tag{10}$$

$0.074 < L_B < 0.214$, $0 < L_{A_1} < 2.04$, and $0 < L_{A_2} < 2.58$ by calculation,

$$\begin{cases} -0.434 < x_C < 0.185, \\ -2.08 < y_C < 2.543. \end{cases} \tag{11}$$

The two boundary unbalances are, respectively, amplitude 2.13 mm/s and phase 103 degrees and amplitude 2.48 mm/s and phase 274 degrees. The predicted phase is 270 degrees and the amplitude is 1.24 mm/s, so a counterweight of 152.3 g is added to the direction of the drum end surface at 90 degrees. Field dynamic balance test of the threshing drum is shown in Figure 16(a), and the measurement results are shown in Table 6.

Remove the mass of hole no. 1 and add it to hole no. 2, the counterweight of the end surface of the drum remains unchanged, and the measurement results are shown in Table 6.

In the second set of experiments, add 161.3 g of trial mass to the 1st hole in the 270-degree direction of the threshing drum, $\mathrm{OB} = (0, -L_B)$.

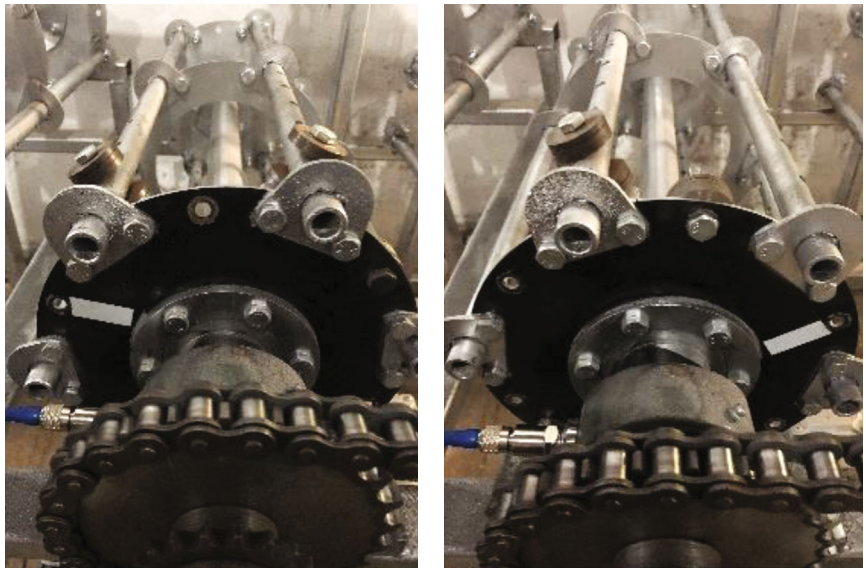

(a) 30-degree rack unbalance test (b) 270-degree rack unbalance test

Figure 16: On-site dynamic balance test of threshing drum.

Table 6: Unbalanced amount before and after the test.

	30 degrees		270 degrees	
	Amplitude (mm/s)	Phase (°)	Amplitude (mm/s)	Phase (°)
Before balancing				
Hole 1	1.587	286	1.264	148
Hole 2	1.487	283	0.943	150
Prediction				
Holes 1, 2	1.24	270	1.4	120
Error				
Hole 1	21.87%	5.6%	9.7%	18.9%
Hole 2	16.6%	4.6%	32.64%	20%
After balancing				
Hole 1	0.731	329	0.59	157
Hole 2	0.682	335	0.453	152

From formulas (3), (4), and (5),

$$\begin{cases} x_C = -L_{A_1} \sin 15^\circ, \\ y_C = -L_B - L_{A_1} \cos 15^\circ + L_{A_2}, \end{cases} \tag{12}$$

$0.074 < L_B < 0.214$, $0 < L_{A_1} < 2.04$, and $0 < L_{A_2} < 2.58$, by calculation,

$$\begin{cases} -0.528 < x_C < 0, \\ -1.9 < y_C < 2.794. \end{cases} \tag{13}$$

The two boundary unbalances are, respectively, amplitude 1.97 mm/s and phase 106 degrees and amplitude 2.79 mm/s and phase 270 degrees. The predicted phase is 120 degrees and the amplitude is 1.4 mm/s, so a counterweight of 165.8 g is added to the direction of the drum end surface at 300 degrees. Field dynamic balance test of the threshing drum is shown in Figure 16(b), and the measurement results are shown in Table 6.

Remove the mass of hole no. 1 and add it to hole no. 2, the counterweight of the end surface of the drum remains unchanged, and the measurement results are shown in Table 6.

It can be seen from Table 6 that the unbalance of the threshing drum predicted by this method is close to the actual measured unbalance. The amplitude of the unbalance of the threshing drum in the first set of tests after one balance is reduced from 1.587 mm/s to 0.731 mm/s. The amplitude in the second group decreases from 1.264 mm/s to 0.59 mm/s, and the change of the unbalanced axial distance has little effect on the rotor balance state.

4. Conclusions

Under the influence of the chain drive, the unbalanced phase of the rotary part is always located in the vicinity of the chain drive equivalent unbalance. For a rotating part with an initial unbalanced phase of 161 degrees, add 58.8 g of mass in its 240-degree direction. Theoretically, the unbalanced phase should be between 161 and 240 degrees. However, the actually measured unbalanced phase is 108 degrees, which is located near the equivalent unbalanced phase (105 degrees) of the tight side of the chain drive.

This paper gives a general method for calculating the equivalent unbalance of the chain drive. The phase of the equivalent unbalance is determined according to the range of the wrap angle of the chain drive and the actual meshing situation. As far as the threshing drum dynamic balance test bench in this article is concerned, the chain drive tight side equivalent unbalance amplitude range is $0 < L_{A_1} < 2.04$ mm/s and the phase angle is 105 degrees, while the loose side equivalent unbalance amplitude range is $0 < L_{A_2} < 2.58$ mm/s and the phase angle is 270 degrees.

The on-site dynamic balancing method based on the side chain drive considers the influence of the chain drive on the balance state of the rotating parts. The unbalance of the threshing drum predicted by this method is smaller than the actual measured unbalance. The maximum error is 32.64%; the minimum error is 4.6%. The amplitude of the unbalance of the threshing drum decreased by 0.856 mm/s and 0.674 mm/s after balancing in the two sets of experiments, and when balanced, the axial distance change of the unbalance can be ignored for the rigid rotor. For the same object, it can be used repeatedly after calculating the equivalent unbalance of the chain drive once.

Data Availability

The data used to support the findings of this study are available from the corresponding author upon request.

Conflicts of Interest

The authors declare that they have no conflicts of interest.

Acknowledgments

This research work was supported by the National Key Research and Development Project 2017YFD0700200.

References

[1] L. Xu, Y. Li, and P. Sun, "Vibration measurement and analysis of tracked-whole feeding rice combine harvester," *Transactions of the Chinese Society of Agricultural Engineering*, vol. 30, no. 8, pp. 49–55, 2014.

[2] A. Donth, A. Grunwald, and C. Heilmann, "Multi-plane on-site balancing of wind turbine drive trains," in *European Wind Energy Conference and Exhibition*, pp. 1940–1946, Copenhagen (DK), 2012.

[3] Z. Gao, L. Xu, Y. Li, Y. Wang, and P. Sun, "Vibration measurement and analysis of tracked rice and wheat combine harvester under field harvesting conditions," *Transactions of the Chinese Society of Agricultural Engineering*, vol. 33, no. 20, pp. 48–55, 2017.

[4] Y. Zhao, R. Tong, and L. Wu, "Research on coupled vibration characteristics of double gearbox transmission system," *Mechanical Transmission*, vol. 42, no. 9, pp. 1–6, 2018.

[5] X. Wang, *Lateral vibration study of chain drive, [M.S. thesis]*, North University of China, Taiyuan, China, 2012.

[6] O. T. Filsoof, M. H. Hansen, A. Yde, P. Bøttcher, and X. Zhang, "A novel methodology for analyzing modal dynamics of multi-rotor wind turbines," *Journal of Sound and Vibration*, vol. 493, article 115810, 2021.

[7] O. A. Polushkin, O. O. Polushkin, and I. M. Fofana, "More efficient balancing of rotors," *Russian Engineering Research*, vol. 37, no. 7, pp. 574–578, 2017.

[8] Z. Tang, H. Zhang, and Y. Zhou, "Unbalanced Vibration Identification of Tangential Threshing Cylinder Induced by Rice Threshing Process," *Shock and Vibration*, vol. 2018, no. Part 5, Article ID 4708730, pp. 1–14, 2018.

[9] Y. Fujiwara, "Analysis of coupled vibration on rotating shaft and supported system," *Bulletin of Kyushu Kyoritsu University Faculty of Engineering*, vol. 29, pp. 9–14, 2005.

[10] X. Yao, "Study on the unbalance response of a rotor on the basis of prestress method," *Journal of Vibration and Shock*, vol. 24, no. 2, pp. 84–86, 2005.

[11] S. Wang, Y. Zi, S. Qian, B. Zi, and C. Bi, "Effects of unbalance on the nonlinear dynamics of rotors with transverse cracks," *Nonlinear Dynamics*, vol. 91, no. 4, pp. 2755–2772, 2018.

[12] M. Tiwari, K. Gupta, and O. Prakash, "Dynamic response of an unbalanced rotor supported on ball bearings," *Journal of Sound and Vibration*, vol. 238, no. 5, pp. 757–779, 2000.

[13] C. Zhao, B. Wen, and X. Zhang, "Synchronization of the four identical unbalanced rotors in a vibrating system of plane motion," *Science China Technological Sciences*, vol. 53, no. 2, pp. 405–422, 2010.

[14] J. Liu, Y. Xu, and G. Pan, "A combined acoustic and dynamic model of a defective ball bearing," *Journal of Sound and Vibration*, vol. 501, article 116029, 2021.

[15] S. B. Zhao, X. M. Ren, W. Q. Deng, K. Lu, Y. Yang, and C. Fu, "A transient characteristic-based balancing method of rotor system without trail weights," *Mechanical Systems and Signal Processing*, vol. 148, article 107117, 2021.

[16] D. Shin and A. Palazzolo, "Nonlinear analysis of a geared rotor system supported by fluid film journal bearings," *Journal of Sound and Vibration*, vol. 475, article 115269, 2020.

[17] J. Deng, *A study on the method for calculating rotational vibration of serpentine belt accessory drive system, [M.S. thesis]*, South China University of Technology, Guangzhou, China, 2015.

[18] Z. Liu, *Research on timing silent chain system dynamics considering the coupled vibration of internal combustion engine system, [M.S. thesis]*, Chongqing University of Technology, Chongqing, China, 2016.

[19] M. G. Donley, T. C. Lim, and G. C. Steyer, "Dynamic analysis of automotive gearing systems," SAE Technical Paper Series, 1992.

[20] A. S. Lee and J. W. Ha, "Maximum unbalance responses of a gear-coupled two-shaft rotor-bearing system," in *Proceedings of the ASME Turbo Expo 2003, collocated with the 2003 International Joint Power Generation Conference. Volume 4: Turbo Expo 2003*, pp. 473–480, Atlanta, GA, USA, 2003.

[21] H. Sun, *Analysis of the imbalance vibration behavior of high-speed spindle and research of its suppression method, [M.S. thesis]*, Xidian University, Xi'an, China, 2015.

[22] Y. Yang, J. Wang, X. Wang, and Y. Dai, "A general method to predict unbalance responses of geared rotor systems," *Journal of Sound and Vibration*, vol. 381, pp. 246–263, 2016.

[23] J. Liu, R. Pang, S. Ding, and X. Li, "Vibration analysis of a planetary gear with the flexible ring and planet bearing fault," *Measurement*, vol. 165, article 108100, 2020.

[24] D. S. Alves, T. H. Machado, K. L. Cavalca, and N. Bachschmid, "Characteristics of oil film nonlinearity in bearings and its effects in rotor balancing," *Journal of Sound and Vibration*, vol. 459, article 114854, 2019.

[25] W. Wang, W. Guo, and H. Tian, "Simulation analysis of lateral vibration characteristics of toothed chain drive system," *Journal of Chengde Petroleum College*, vol. 17, no. 1, pp. 25–27, 2015.

[26] W. Qin, "Analysis of lateral vibration stability of roller chain drive," *Journal of Mechanical Transmission*, vol. 34, no. 8, pp. 79–82+91, 2010.

[27] C. Pereira, J. Ambrósio, and A. Ramalho, "Application of a tensioner on a chain drives multibody model," *Applied Mechanics and Materials*, vol. 394, pp. 140–143, 2013.

[28] D. Li, D. Chu, and H. Ding, "The frequency-response curve of a belt-drive system by using the harmonic balance method," *Journal of Dynamics and Control*, vol. 13, no. 6, pp. 424–430, 2015.

[29] V. A. Bazhenov, O. O. Lukyanchenko, Y. V. Vorona, and O. Kostina, "Dynamic stability of elastic systems parametric oscillations," *Opir Materialiv I Teoria Sporud-Strength Of Materials And Theory Of Structures*, vol. 95, pp. 159–186, 2015.

[30] K. W. Wang, "On the stability of chain drive systems under periodic sprocket oscillations," *Journal of Vibration and Acoustics*, vol. 114, no. 1, pp. 119–126, 1992.

[31] H. Diken and K. Alnefaie, "Effect of unbalanced rotor whirl on blade vibrations," *Journal of Sound and Vibration*, vol. 330, no. 14, pp. 3498–3506, 2011.

[32] X. Wang, J. Gao, and X. Zhang, "Lateral vibration analysis of roller chain drive under the influence of gravity," *Mechanical Research & Application*, vol. 24, no. 2, pp. 28–30+40, 2011.

[33] J. Yang, X. Feng, and L. Zhao, "Influences of belt drive on the rotor balance detection system," *Journal of Convergence Information Technology*, vol. 7, no. 23, pp. 672–679, 2012.